

Shock Wave Emissions of a Sonoluminescing Bubble

Joachim Holzfuss, Matthias Rüggeberg, and Andreas Billo

Institut für Angewandte Physik, TU Darmstadt, Schloßgartenstraße 7, 64289 Darmstadt, Germany

(Received 7 August 1998)

A single bubble in water is excited by a standing ultrasound wave. At high intensity the bubble starts to emit light. Together with the emitted light pulse, a shock wave is generated in the liquid at collapse time. The time-dependent velocity of the outward-traveling shock is measured with an imaging technique. The pressure in the shock and in the bubble is shown to have a lower limit of 5500 bars. Visualization of the shock and the bubble at different phases of the acoustic cycle reveals previously unobserved dynamics during stable and unstable sonoluminescence. [S0031-9007(98)07896-X]

PACS numbers: 78.60.Mq, 42.65.Re, 43.25.+y

When intense ultrasound is applied to water, bubbles appear in the liquid. Among the properties they exhibit is sound radiation and emission of photons [1]. In a controlled experiment, a single bubble alone may be driven stably in a standing ultrasound field. Here, intense light pulses of very short duration may be observed. Since this discovery [2] experimental work on the so-called single bubble sonoluminescence (SBSL) has been extensively carried out to explain the phenomenon and the interesting features it displays: The energy is focused by 12 orders of magnitude [3], the light pulses are of picosecond duration [4], the emitted light energy per pulse is in the MeV range, and the blackbodylike spectrum peaks in the ultraviolet. The interpulse synchronicity can be accurate on the picosecond scale [3] or chaotic on the microsecond scale [5]. Parameter studies have been done showing the region of stable SBSL lying on the boundary of a dissolution island [6]. Advanced driving of the bubble is employed to increase the light output [7]. Theoretical and numerical work [8–10] has been done to explain SBSL but so far few basic assumptions of the different theories could be verified experimentally. An inner shock wave launched in the interior of the bubble upon collapse has theoretically been assumed to account for the observed short SBSL light pulse and its spectrum [9,11,12].

Our experimental and numerical work focuses on the observation of shock waves being emitted into the liquid at bubble collapse [13]. The shock waves are visualized, the velocity of the front as it travels outwards is measured, and the peak pressure of the shock is deduced. Effects appearing at unstable SBSL are analyzed. The experiments are consistent with numerical simulations. In the experiment (Fig. 1) the standing ultrasound wave is produced in a cylindrical cell filled with water of ambient temperature, distilled, and degassed to 10%–40% of ambient gas pressure. The cell consists of two piezoceramic cylinders connected by a glass tube [14] of 2.9 cm radius (overall height 12 cm). An optical glass plate closes the bottom, and the top remains open. The driving frequency is 23.5 kHz and the driving amplitude is ≈ 1.2 to 1.5 bars. A bubble is inserted into the liquid with a syringe. The

oscillating bubble is illuminated from the top by a copper vapor laser by light pulses of 7 ns duration (FWHM) followed by a low intensity tail of 30 ns. The wavelength is 511 nm. The repetition rate of one-half the driving frequency is adjusted via a controllable delay to accommodate locking to the driving signal at a preset phase.

Because shock waves modulate the phase of the laser light, optical filtering is used to transform this information into intensity modulations. Therefore the bubble image is passed through a (magnifying) $4f$ spatial Fourier filter. Specifically, a dark-ground method [15] is used that removes the zeroth order in the Fourier plane with a thin metal stick. Subsequently the image is picked up by a video camera delivering 25 frames/s. The shutter opening time is 0.25 ms such that the average image of 2–3 shock waves is seen. Because of the stable repetitive bubble collapse a slow motion video of the oscillations [14,16] and the shedding of shock waves is produced by slightly detuning the laser flash frequency. The images of the shock waves are digitized in a computer, and their radius/time curves can be plotted. Because of their submicron size, sonoluminescing bubbles are hard to detect at collapse. But by recording the center of the shock wave the bubble position can be determined. Figure 2 shows the images of shock waves at different times. The shock is emitted at the main collapse of the bubble. The shock front shows

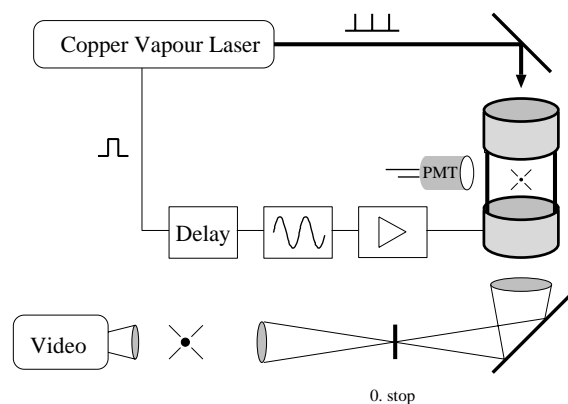


FIG. 1. Experimental setup.

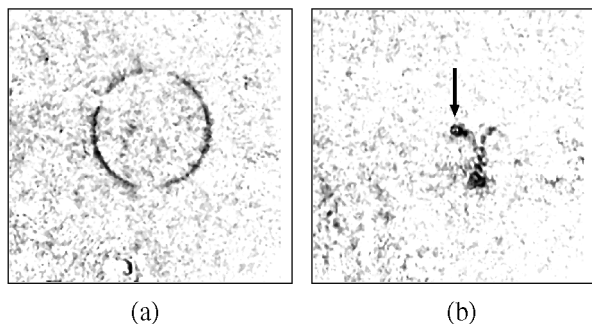


FIG. 2. Images of shock waves emitted by a sonoluminescing bubble. (a) At $t = 480$ ns after collapse. (b) Reflection from the side walls at $t = 3.54 \mu\text{s}$ before collapse. The arrow marks the bubble position; image side length is 3.5 mm.

up as a circle (Fig. 2a) and no anisotropy is seen within the optical resolution limit of $1.5 \mu\text{m}$, which is an indication of a symmetrical collapse. The front proceeds to the outer glass wall of the cylinder, reflects, and moves inward again. The reflected shock wave has a duration >40 ns and is distorted, presumably due to imperfections or misalignment of the glass wall. Figure 2b shows the shock wave at the time it is refocused the most ($3.54 \mu\text{s}$ before the next collapse). The main pressure peak seems to be $\approx 700 \mu\text{m}$ away from the bubble at the lower end of a line structure. The refocused shock is sometimes powerful enough to kick the bubble through space a bit as it passes it. Weaker secondary reflections are also observable. At no time we could see a pressure pulse due to bubble rebounds [17]. The duration of the shock pulse can be determined to be 10 ns (FWHM). As this is on the order of the optical pulse length of 7 ns, this value is an upper bound.

From successive images the velocity of the shock front is calculated. Figure 3 shows the average velocities as a function of distance from the bubble center. At very small distances ($6\text{--}73 \mu\text{m}$) an average value of $\bar{v} = 2000$ m/s is measured; at larger distances the velocity of the shock front is decreasing to the ambient sound speed. Because the velocity of the shock decreases rapidly, the instantaneous velocity may be well above 2000 m/s. The pressure p in the shock can be determined from its velocity v by a Rankine-Hugeniot relation [18] and a state equation for water, namely, the Tait equation

$$v = \frac{1}{\rho_0} \sqrt{\frac{p - p_0}{\rho_0^{-1} - \rho^{-1}}} \quad \text{and} \quad \frac{p + B}{p_0 + B} = \left\{ \frac{\rho}{\rho_0} \right\}^n. \quad (1)$$

ρ and p are the maximal density and pressure in the shock, $\rho_0 = 998.2 \text{ kg/m}^3$ and $p_0 = 1$ bar are the ambient density and pressure, $n = 7.025$, and $B = 3046$ bars [19]. Using (1), the shock pressure can be calculated to be 5500 bars.

Numerical calculations have been carried out to further analyze the time dependence of the velocity and pressure of the shock front. The Gilmore model [20] describing the radial motion of a bubble is used.

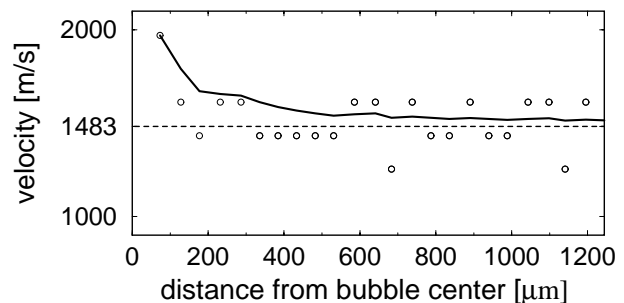


FIG. 3. Average velocities ($t_{\text{avg}} = 34$ ns) of the SBSL-shock wave from successive images as a function of the distance from the generation (circles). The solid line is the mean velocity extrapolated by averaging over all measurement points up to a respective distance r from the bubble center.

$$\begin{aligned} \left(1 - \frac{\dot{R}}{C}\right) R \ddot{R} + \frac{3}{2} \left(1 - \frac{\dot{R}}{3C}\right) \dot{R}^2 \\ = \left(1 + \frac{\dot{R}}{C}\right) H + \left(1 - \frac{\dot{R}}{C}\right) \frac{R}{C} \frac{dH}{dt}, \end{aligned} \quad (2)$$

$$\begin{aligned} C = c|_{r=R} = \sqrt{\frac{dp}{d\rho}} \Big|_{r=R} = c_0 \left(\frac{p(R, \dot{R}) + B}{p_0 + B} \right)^{(n-1)/2n}, \\ p(R, \dot{R}) = \left(p_0 + \frac{2\sigma}{R_0} \right) \left(\frac{R_0^3 - a^3}{R^3 - a^3} \right)^\kappa \\ - \frac{2\sigma}{R} - \frac{4\mu}{R} \dot{R}. \end{aligned}$$

R is the bubble radius, C , ρ , and p are the speed of sound in the liquid, its density, and the pressure at the bubble wall, respectively. $H = \int_{p_\infty}^{p(R)} \rho^{-1} dp$ is the enthalpy of the liquid. Parameters were set to $c_0 = 1483$ m/s, $\sigma = 0.0725$ N/m, and $\mu = 0.001$ N s/m³. $a = R_0/8.86$ is a hard-core van der Waals term [21] and $\kappa = 5/3$ the adiabatic exponent for argon [10]. The pressure at infinity is $p_\infty = p_0 + p_e \cos(2\pi ft)$, and p_e and f are the driving pressure and frequency.

The dynamics of the pressure pulse in the liquid is calculated by using the Kirkwood-Bethe hypothesis [20]: the invariant quantity $Y = R(H + \frac{1}{2} \dot{R}^2)$ propagates with the characteristic velocity $c + u$, the local sound plus particle velocity in the liquid. The outgoing characteristics are determined by [22]

$$\begin{aligned} \frac{du}{dt} &= \frac{1}{c - u} \left[(c + u) \frac{Y}{r^2} - \frac{2c^2 u}{r} \right], \\ \frac{dp}{dt} &= \frac{\rho_0}{r(c - u)} \left(\frac{p + B}{p_0 + B} \right)^{1/n} \left[2c^2 u^2 - \frac{c(c + u)}{r} Y \right]. \end{aligned}$$

Solving the bubble equation (2) gives the initial values R , \dot{R} , H , and $u = \dot{R}$ for each characteristic. Crossing characteristics in r - t space imply the generation of a shock. The exact position of the shock front can be

obtained by equalization of the particle velocities in the hysteretic $u-t$ curves [23].

Figure 4 shows the calculated shock wave velocity as a function of the distance from the bubble center. The maximal velocity of the pressure peak of approximately 8300 m/s decreases within the first 100 μm to the ambient sound velocity. For comparison with the experiment the mean velocity of the peak is shown in Fig. 4. The experimentally obtained short time average and mean velocities compare quite well to the numerical findings. The particle velocity in the model reaches a maximum value of 333 m/s. The inset of Fig. 4 shows the peak pressure of the shock as it travels away from the center. The maximum value of 73 000 bars at 1 μm decays quickly with increasing distance, within 100 μm with a faster decay rate than the usual r^{-1} . Though these numbers may be somewhat overestimated due to model limitations, it is seen that within the first few μm extreme conditions exist in the fluid. The greater dissipation close to the bubble may account for differences between our experimental results and previous inferences of the shock pressure from direct hydrophone measurements, which have yielded smaller values for the pressure [17,24].

Using the shock wave as a microscope for the bubble position at collapse time, the time dependence and the position of the collapse have been measured for unstable SBSL. Unstable SBSL occurs at the upper parameter values of the driving pressure and ambient gas concentration: The ambient bubble radius grows until the bubble dynamics reaches an instability where bubble volume is rapidly lost. This cycle repeats itself on a slow time scale [2,25]. Using rare events of double exposure at split-off time, the

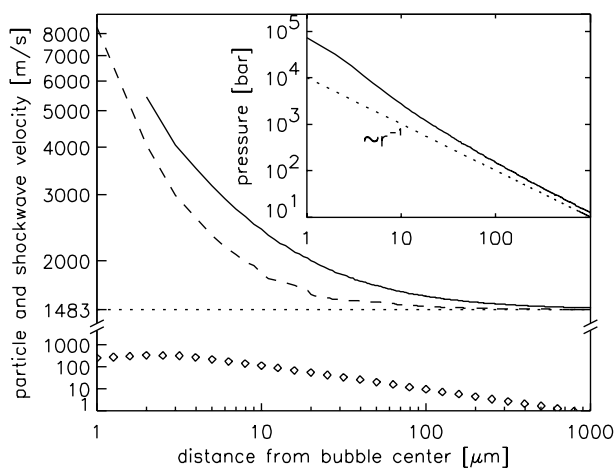


FIG. 4. Numerical calculations of a shock wave generated at collapse time of a bubble of 5 μm ambient radius driven at 23.5 kHz and 1.45 bars. Shown are data for the pressure peak that is traveling away from the bubble into the liquid as a function of distance from the bubble center. Dashed line: velocity of the peak; solid line: extrapolated mean shock velocity; squares: particle velocity. The inset shows the calculated peak pressure in the shock as a function of distance from the bubble (solid line). The dotted line shows a r^{-1} reference line for comparison.

distance of the centers of two shock waves representing a bubble before and after the split-off can be used to calculate a lower bound of the bubble velocity due to the recoil of 0.5 m/s. During unstable SBSL the bubble shows its dynamical behavior over a long range of its ambient radius as a parameter. Figure 5 shows the radius of the shock wave and the bubble position at collapse time as a function of time. All experimental conditions were kept constant. It is seen that the bubble collapse does not occur at a constant phase any more. As the ambient bubble radius grows by diffusion, the collapse is shifted to later times. Because the illuminating flash occurs at a fixed phase of the driving signal some small time after the collapse, a later collapse decreases the time the shock front can travel outward until it is imaged. This way a larger ambient bubble radius shows up as a smaller shock radius. In Fig. 5a the recurrent process of growing on a slow time scale and a subsequent rapid decrease of ambient volume of the bubble is seen. At split-off the collapse time of the bubble is shifted by $\approx 1 \mu\text{s}$ with respect to the driving phase. Calculations of collapse time vs bubble volume for

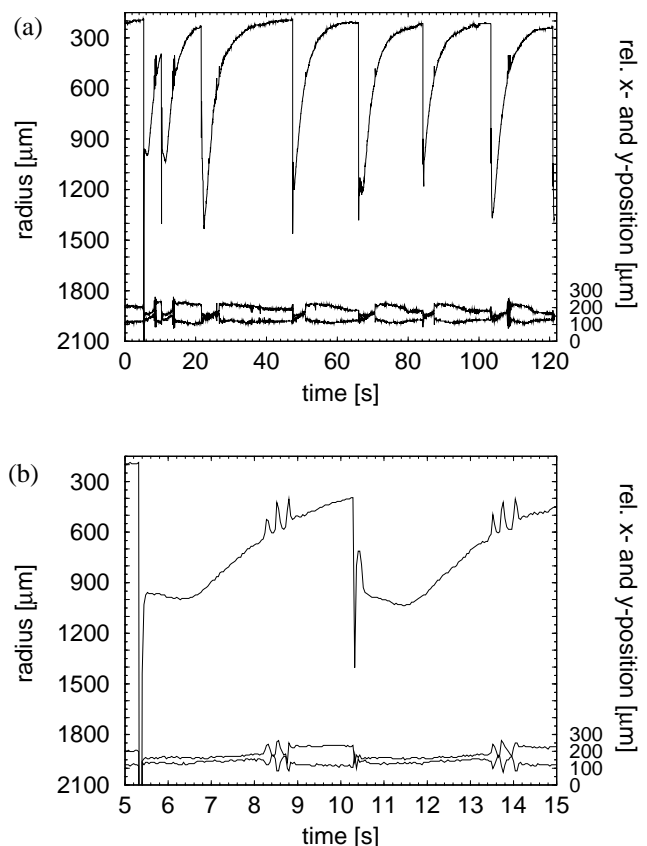


FIG. 5. Measured radii of shock waves and position of the center during unstable SBSL. Data have been digitized from images taken each 40 ms at a constant phase of the driving. (a) The upper line shows the radii of shock waves as a function of time, as they change on a slow time scale. The lower two lines are relative x and y coordinates of the bubble at collapse. (b) Zoom into the first seconds of (a). Spatial oscillations are seen as the shock radii (and the ambient radius of the bubble) are changing at, e.g., $t = 8-9$ s.

SBSL-relevant bubble radii show (see also [2]) that the bubble loses about one half of its volume. Most probably, multiple fragments (microbubbles) will be generated. So far microbubbles have been observed at the lower amplitude threshold of SBSL, where they have a slowly decreasing velocity of initially 3–4 mm/s, do not return to the bigger bubble, but dissolve within a few hundred μm within ≈ 0.1 s. A closer look on a single cycle of Fig. 5 reveals that the growing phase has a peculiar fine structure. Immediately after microbubble split-off (e.g., at $t = 5.4, 10.4$ s) the collapse is shifted to later times (smaller shock radii), reaching a slightly decreasing plateau until it finally increases. During each growing phase small bumps are seen (e.g., at $t = 8\text{--}9$ s). Looking at the position of the bubble one sees a connection: Each time the phase bumps, the bubble moves discretely through space and finally settles. The explanation may be oscillation in different resonances, shock wave interaction, or the acoustic field acting on the bubble is altered as it grows.

We have visualized the generation of shock waves from a sonoluminescing bubble for the first time. Resulting from the enormous pressure inside the bubble and the great amount of energy transported by the surrounding liquid, the shock front is shown to have a faster speed than the ambient sound velocity. If one calculates [26] the change in the refractive index of water due to the theoretical local overpressure of 73 kbar, one arrives at a $\Delta n = 0.23$, which is 70% of the change at an air/water interface. Therefore measurements of the minimal radius by Mie scattering together with statements about the exact timing of the flash with respect to the minimal radius should be done keeping this in mind as the shock wave builds a scattering layer around the bubble. We cannot conclude from our data whether the visualized shock in the liquid also consists of contributions of an hypothetical inner bubble shock that may be responsible for SBSL. The observed refocused shock can be shown to have an impact on the bubble dynamics. It would be interesting to see if exact positioning and control of the timing of the reflected shock wave can be used to increase SBSL intensity [7,9].

The authors thank R.G. Holt for continuous collaboration, R.A. Roy and T.J. Matula for discussions, S.J. Putterman for stimulating questions, and the TU Darmstadt for making the research possible. The work has been funded through the SFB 185 "Nichtlineare Dynamik" of the DFG.

-
- [1] T.G. Leighton, *The Acoustic Bubble* (Academic Press, London, 1994); W. Lauterborn and J. Holzfuss, *J. Bifurcation Chaos* **1**, 13 (1991).
 [2] D.F. Gaitan, L.A. Crum, C.C. Church, and R.A. Roy, *J. Acoust. Soc. Am.* **91**, 3166 (1992).
 [3] B.P. Barber, R.A. Hiller, R. Löffstedt, S.J. Putterman, and K.R. Weninger, *Phys. Rep.* **281**, 65 (1997).
 [4] B.P. Barber and S.J. Putterman, *Nature (London)* **352**, 318 (1991); B. Gompf, R. Günther, G. Nick, R. Pecha, and W. Eisenmenger, *Phys. Rev. Lett.* **79**, 1405 (1997);

- R.A. Hiller, S.J. Putterman, and K.R. Weninger, *Phys. Rev. Lett.* **80**, 1090 (1998); M.J. Moran and D. Sweider, *Phys. Rev. Lett.* **80**, 4987 (1998).
 [5] R.G. Holt, D.F. Gaitan, A.A. Atchley, and J. Holzfuss, *Phys. Rev. Lett.* **72**, 1376 (1994).
 [6] R.G. Holt and D.F. Gaitan, *Phys. Rev. Lett.* **77**, 3791 (1996).
 [7] J. Holzfuss, M. Rüggeberg, and R. Mettin, *Phys. Rev. Lett.* **81**, 1961 (1998).
 [8] L. Frommhold and A.A. Atchley, *Phys. Rev. Lett.* **73**, 2883 (1994).
 [9] W.C. Moss, D.B. Clarke, J.W. White, and D.A. Young, *Phys. Lett. A* **211**, 69 (1996); W.C. Moss, D.B. Clarke, and D.A. Young, *Science* **276**, 1398 (1997).
 [10] A chemical dissociation theory states that only argon remains within sonoluminescing air bubbles. See D. Lohse, M. Brenner, T. Dupont, S. Hilgenfeldt, and B. Johnston, *Phys. Rev. Lett.* **78**, 1359 (1997) for the theory and T.J. Matula and L.A. Crum, *Phys. Rev. Lett.* **80**, 865 (1998) for an indirect experimental evidence (also [6]).
 [11] R.A. Hiller, S.J. Putterman, and K.R. Weninger, *Phys. Rev. Lett.* **80**, 1090 (1998).
 [12] C.C. Wu and P.H. Roberts, *Phys. Rev. Lett.* **70**, 3424 (1993).
 [13] J. Holzfuss, M. Rüggeberg, and A. Billo, *Fortschritte der Akustik—DAGA 97* (DPG GmbH, Bad Honnef, 1997), pp. 341–342.
 [14] R.G. Holt, J. Holzfuss, A. Judt, A. Phillip, and S. Horsburgh, in *Frontiers of Nonlinear Acoustics: Proceedings of the 12th ISNA*, edited by M.F. Hamilton and D.T. Blackstock (Elsevier Science, London, 1990), pp. 497–502.
 [15] E. Hecht, *Optics* (Addison-Wesley, Reading, MA, 1987).
 [16] Y. Tian, J.A. Ketterling, and R.E. Apfel, *J. Acoust. Soc. Am.* **100**, 3976 (1996).
 [17] T.J. Matula, I.M. Hallaj, R.O. Cleveland, L.A. Crum, W.C. Moss, and R.A. Roy, *J. Acoust. Soc. Am.* **103**, 1377 (1998).
 [18] P.M. Morse and K.U. Ingard, *Theoretical Acoustics* (Princeton University Press, Princeton, 1968).
 [19] The constants n and B stem from fits of the C/p relation [in Eq. (2)] to data from E.W. Lemmon, M.O. McLinden, and D.G. Friend, in *NIST Chemistry WebBook*, NIST Stand. Ref. Database Number 69, edited by W.G. Mallard and P.J. Linstrom (NIST, Gaithersburg, MD, 1998) (<http://webbook.nist.gov>).
 [20] R.T. Knapp, J.W. Daily, and F.G. Hammit, *Cavitation* (McGraw-Hill, New York, 1970).
 [21] R. Löffstedt, B.P. Barber, and S.J. Putterman, *Phys. Fluids A* **5**, 2911 (1993).
 [22] Y.-P. Lee, S.W. Karng, J.-S. Jeon, and H.-Y. Kwak, *J. Phys. Soc. Jpn.* **66**, 791 (1997).
 [23] O.V. Rudenko and S.I. Soluyan, *Theoretical Foundations of Nonlinear Acoustics* (Consultants Bureau, New York, 1977), p. 28.
 [24] K.R. Weninger, B.P. Barber, and S.J. Putterman, *Phys. Rev. Lett.* **78**, 1799 (1997).
 [25] B.P. Barber, K. Weninger, R. Löffstedt, and S.J. Putterman, *Phys. Rev. Lett.* **74**, 5276 (1995).
 [26] $[(n_r^2 - 1)/(n_r^2 + 2)]\rho^{-1} = 0.2060 \times 10^{-3} \text{ m}^3/\text{kg}$ and Eq. (1), from H. Schardin, *Erg. exakt. Naturwiss.* **20**, 370 (1942).